IOP Publishing | Royal Swedish Academy of Sciences Physica Scripta

Phys. Scr. **90** (2015) 108005 (15pp) doi:10.1088/0031-8949/90/10/108005

Invited Comment

Models for the probability densities of the turbulent plasma flux in magnetized plasmas

A S Bergsaker[1], Å Fredriksen[2], H L Pécseli[1] and J K Trulsen[3]

[1] University of Oslo, Physics Department, PO Box 1048 Blindern, N-0316 Oslo, Norway
[2] University of Tromsø, Department of Physics and Technology, N-9037 Tromsø, Norway
[3] University of Oslo, Institute for Theoretical Astrophysics, PO Box 1029 Blindern, N-0315 Oslo, Norway

E-mail: hans.pecseli@fys.uio.no

Received 23 March 2015, revised 3 July 2015
Accepted for publication 11 August 2015
Published 18 September 2015

Abstract

Observations of turbulent transport in magnetized plasmas indicate that plasma losses can be due to coherent structures or bursts of plasma rather than a classical random walk or diffusion process. A model for synthetic data based on coherent plasma flux events is proposed, where all basic properties can be obtained analytically in terms of a few control parameters. One basic parameter in the present case is the density of burst events in a long time-record, together with parameters in a model of the individual pulse shapes and the statistical distribution of these parameters. The model and its extensions give the probability density of the plasma flux. An interesting property of the model is a prediction of a near-parabolic relation between skewness and kurtosis of the statistical flux distribution for a wide range of parameters. The model is generalized by allowing for an additive random noise component. When this noise dominates the signal we can find a transition to standard results for Gaussian random noise. Applications of the model are illustrated by data from the toroidal Blaamann plasma.

Keywords: plasma turbulence, turbulent transport, statistical analysis

(Some figures may appear in colour only in the online journal)

1. Introduction

Most plasmas confined by magnetic fields exhibit strong fluctuations, in particular at the steep gradients near the plasma edge. These fluctuations are due to plasma instabilities and often give rise to anomalous transport in toroidal [1, 2] as well as linear devices [3]. Because of the importance of this problem, these fluctuations have been studied intensively both experimentally, numerically and by analytical methods. Considering the random or turbulent nature of these phenomena a significant part of the analysis has been based on statistical methods. In the present work we use data from the Blaamann experiment [2] for illustrating a randomly varying plasma flux signal.

The information in the amplitude probability density of a fluctuating quantity is not always easy to estimate due to finite record lengths, and reduced levels of information can be more attractive. Examples are the lowest order statistical moments. A number of observations of low frequency turbulence in magnetized plasmas have demonstrated a systematic relationship between skewness S and kurtosis K of the probability density of some fluctuating quantity [4–8], the density for instance. Earlier, similar relations have been noted and studied for a variety of conditions for neutral atmospheric turbulence [9–14] where local concentrations of contaminants were analyzed. It is often found that the skewness–kurtosis relations associated with these data can be modeled by a parabolic expression like

$$K = AS^2 + C \tag{1}$$

with suitably chosen constants A and C. These processes are often inherently non-Gaussian. For the Gaussian case the

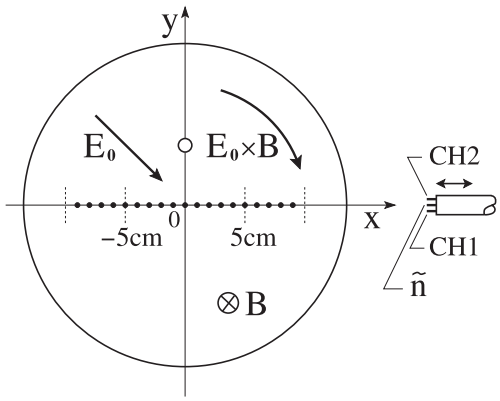

Figure 1. Schematic illustration of the positions for data acquisition by the moving probe in a cross section of the Blaamann torus. One electric field component is obtained from the potential difference between probes CH1 and CH2 on the movable probe. Positions for data acquisition are shown with small filled circles along the x-axis. An open circle shows the position of a fixed reference probe detecting floating potential. The orientation in the figure used here differs from one used previously [20].

relation reduces to a point $(S, K) = (0, 3)$, where we use the definitions

$$S \equiv \frac{\int (\zeta - \langle\zeta\rangle)^3 P(\zeta)\mathrm{d}\zeta}{\sigma^3}$$

$$K \equiv \frac{\int (\zeta - \langle\zeta\rangle)^4 P(\zeta)\mathrm{d}\zeta}{\sigma^4}$$

with $\sigma^2 \equiv \int (\zeta - \langle\zeta\rangle)^2 P(\zeta)\mathrm{d}\zeta$ and $\langle\zeta\rangle \equiv \int \zeta P(\zeta)\mathrm{d}\zeta$, and where ζ is the randomly varying quantity and $P(\zeta)$ is its probability density. Other definitions of K subtract the Gaussian value 3, so that $K \neq 0$ measures deviations from the Gaussian value. It is often found that the analytical form (1) is robust, but the parameters A and B can change with changing experimental conditions. A general model thus has to include some parameters that can account for some essential experimental parameters.

Skewness–kurtosis relations have been discussed by several authors for a number of observations of plasma fluctuations [15, 16]. Several of these discussions have been limited to empirical models of the probability densities, and not to the underlying physical processes. Similar discussions have been presented also for concentration fluctuations in turbulent atmospheres [11], where parameters of a general probability density model are associated with physical processes. The present study describes a model based on the assumption that coherent structures are present in plasma turbulence. We obtain relations between the parameters determining pulse-shapes and the coefficients entering the relation between skewness and kurtosis. By including an additive random noise component we can demonstrate a continuous transition to the Gaussian limit $(S, K) = (0, 3)$ when the random Gaussian noise dominates the signal.

From the outset, from small enough S, it could be argued that a polynomial relation between K and S can be expected. Such a relation can be truncated to second order: $K(S) = AS^2 + DS + C$, with the parameters A, D, and C depending on the context. For a one-parameter scan of any given model or of a set of experimental data, there must be only one curve, since S itself can be used as a parameter. The difference between a generic parabola and (1) is that $D = 0$, or more generally the fact that $K(S)$ is an even function of S. The observations give, however, support for (1) also for large S-values, so an argument based on a series expansion is difficult to maintain. The symmetry, or near symmetry, of K for varying S is a significant constraint that has to be consistent with models. Skewness–kurtosis relations will here be discussed in terms of parametric representations as $(S, K) = (S(\xi), K(\xi))$ where ξ is some model parameter or a set of such parameters. In an experiment ξ can represent a spatial position, for instance, where turbulence conditions vary with this position.

The reduced information in a model relation like (1) can be restrictive and within some uncertainty level be consistent with several models based on different physical assumptions. More general basic features such as the probability densities for fluctuating quantities can offer a better support for a model if they agree favorably with observations. The models developed in this work are based on probability densities built upon physical models for flux signals.

The present paper is organized as follows. In section 2 we present some basic features of the fluctuating flux signal observed in the magnetized toroidal plasma experiment Blaamann at the University of Tromsø [2, 17]. These data form our basic reference case, and serve as representative also for other experimental conditions. Section 3 contains a discussion of properties of a simple analytical model for the flux signal. One of the consequences of this model is a prediction of a relation in the form (1). Finally, section 4 contains our conclusions. The appendix describes a model for synthetic data that can reproduce some of the properties of flux signals found in the literature.

2. Experimental results from the Blaamann torus

As an illustration of the properties of plasma flux data, their skewness–kurtosis relations in particular, we use data from the discharge plasma in the magnetized Blaamann torus. The major radius of the vacuum vessel is $R_0 = 0.67$ m and the minor radius $r_0 = 0.135$ m. The toroidal magnetic field was 1540 G at a reference position in the center of the vacuum vessel. There is no toroidal current nor poloidal magnetic fields imposed on the plasma, and hence no poloidal transform. A small vertical magnetic field is imposed by external coils. The present experiment [18] was carried out in helium gas at a pressure of 1.0×10^{-3} mbar and a discharge current of approximately 1 A. The hot filament was biased at −140 V with respect to the walls. The degree of ionization induced by the discharge is typically ∼1%. The hot filament emits electrons in abundance, and the plasma is electron rich, with a deep negative, nearly parabolic dc potential profile. The plasma conditions depend on the imposed potentials and magnetic fields [19]. Data are collected by movable Langmuir

probes as illustrated in figure 1. The signals were digitized with a 12 bit digitizer at a sampling rate of 250 kHz (i.e. a sampling time of $\Delta t = 4 \times 10^{-6}$ s) and 10^4 samples per channel. Five data records are obtained for each combination of movable (from $x = -9$ to $x = +9$ cm) and reference probe positions. Data similar to those analyzed here were described elsewhere [18, 20] where turbulent plasma fluxes due to low frequency electrostatic fluctuations were analyzed. Inspection of the data demonstrated that the flux signal was characterized by distinct 'spikes' with randomly distributed amplitudes. Similar data samples from the TJ-I tokamak, for instance, have been reported [21].

In a part of the analysis, also data from a similar experiment with argon have been used for comparison. The argon data were obtained with magnetic fields in a range of 440–2640 Gauss, and at two different pressures, 1.0×10^{-4} and 1.0×10^{-3} mbar. The data were acquired at the same rate and record length, but with only one record per x-position. The positions overlapped with those of the helium experiment.

The low frequency fluctuating plasma velocity component in the direction perpendicular to the magnetic field, $\mathbf{B}$, can for these conditions be approximated by the fluctuating $\tilde{\mathbf{E}} \times \mathbf{B}/B^2$-velocity. Signals for fluctuating electric field components and fluctuating plasma densities were available. From these signals the fluctuating component of the plasma flux in the radial direction of the plasma column can be estimated as a product of the density and the radial velocity-component. The estimate is restricted by ignoring for instance the ion polarization drift, which is small, however, since the relevant frequencies are much smaller than the ion cyclotron frequency. The plasma flux is fluctuating with a nonzero mean, indicating a net turbulent transport out of the plasma column. This plasma loss is found to be caused mostly by bursting events as in some other related studies [22]. Since the plasma flux is composed of a product of fluctuating density and velocity, we note that an outward burst can be obtained by the product of two positive or two negative components [20]. Although the two cases contribute with flux structures having the same sign, they will have different temporal and spatial properties. This observation implies that a flux signal can be modeled best by invoking a minimum of two structure shapes.

2.1. Basic features of the data

Details of the toroidal Blaamann device are given elsewhere [2, 17, 20]. The position of the discharge filament used in the present experiment gives a nearly rotationally symmetric parabolic potential variation that enhances the plasma confinement, see figure 2. A sample figure showing a selected cross section is given elsewhere [20], where the shear in rotation velocity at $|x| > 5$ cm is evident. The positioning of the electron emitting filament is essential for the spatial variation of the steady state potential variation. Other experiments place the filament closer to the wall of the device and consequently find a different potential variation. The most important probe information relevant for the discussion in the present analysis is summarized in figure 1. By a movable multi-probe, simultaneous records of fluctuating plasma density and one electric field component were obtained. The electric field is deduced from the potential difference between two closely separated probe tips. A sample of raw data are shown in figure 3. While the fluctuations in density and the radial velocity component have a wide band character, the flux signal has a noticeable component of burst-like structures with a preferred polarity giving a net flux out of the plasma column.

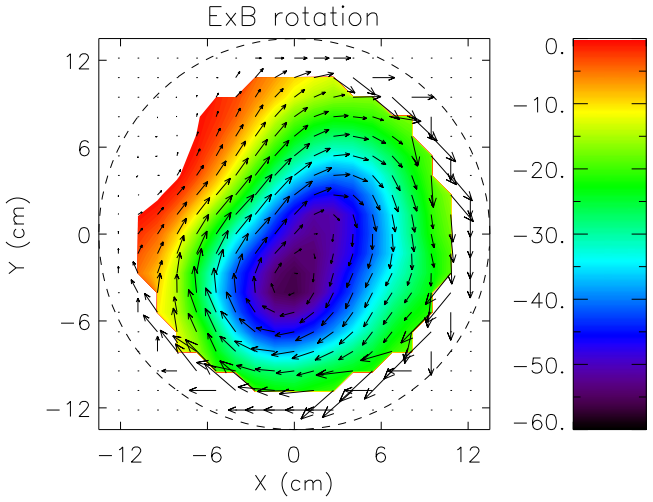

Figure 2. Langmuir probe measurement of the plasma potential in a plasma cross section in a helium discharge. Arrows show the relative magnitude of the average steady state plasma velocity vectors. The color scale to the right of the figure is in volts.

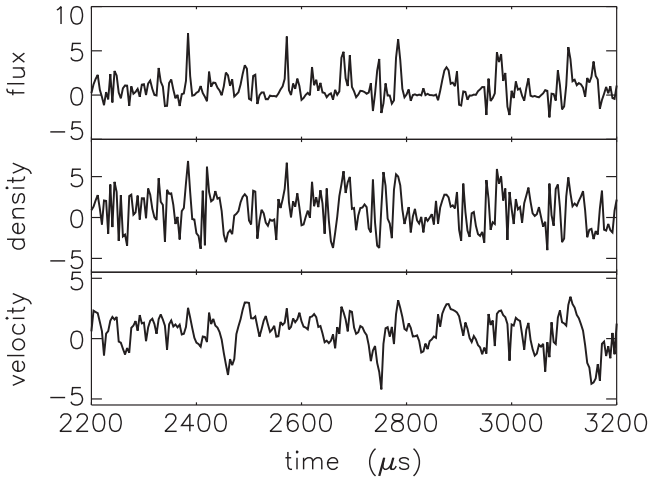

Figure 3. Samples of raw data for fluctuations in the x-component of the plasma flux, plasma density, and the x-component of the $\mathbf{E} \times \mathbf{B}/B^2$-velocity, all obtained at $x = 5$ cm, as functions of time.

The probability densities of the fluctuating quantities, the joint probability densities in particular, can be estimated experimentally, with samples shown in figure 4. Under stationary conditions, the radial component of the plasma flux probability density functions (PDF's) for the same two positions are shown in figure 5. The average plasma flux integrated over a surface with radius R measured with respect to

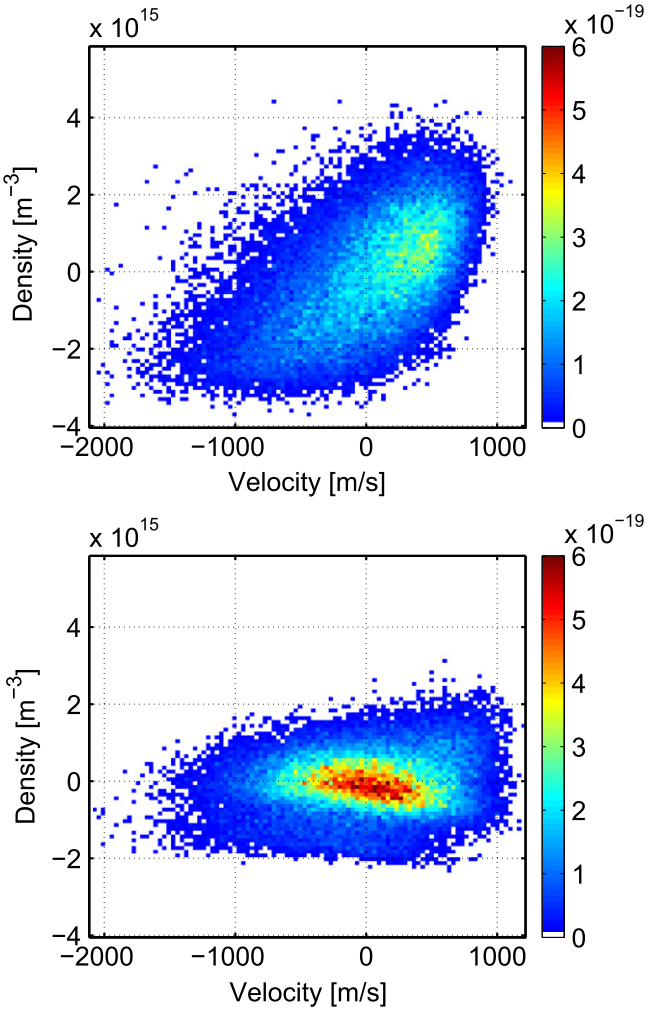

Figure 4. Samples of joint probability densities of fluctuating density and the x-component of the fluctuating plasma velocity as estimated by the x-component of the $\widetilde{\mathbf{E}} \times \mathbf{B}/B^2$-velocity. Results for two positions are shown: $(x,\ y) = (4,\ 0)$ cm (top) and $(x,\ y) = (9,\ 0)$ cm (bottom). For comparison with the observed fluctuating velocities we have the ion sound speed $C_s \approx 10^4$ m s^{-1} for helium plasma at $T_e \approx 5$ eV. The root mean square relative density fluctuations are approximately 10%.

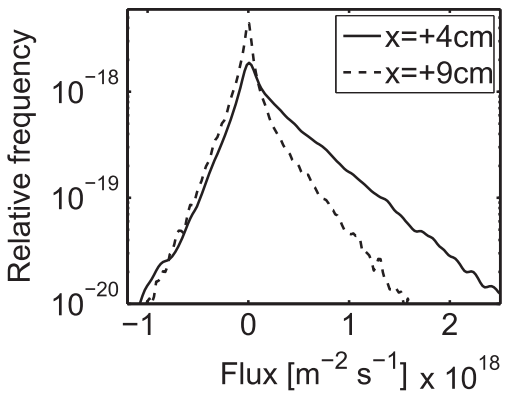

Figure 5. Flux probability densities for two x-positions corresponding to those used in figure 4.

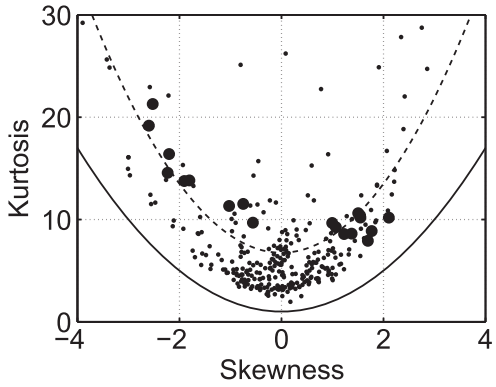

Figure 6. Scatter plot for skewness and kurtosis obtained at the spatial sampling positions of the flux signal. Large filled circles refer to the data for helium used in the present study, while the small dots are for an argon plasma. For reference we show the relation $K = S^2 + 1$ with full line. The dashed line shows the best fit for the helium data, $K = 1.7S^2 + 6.8$. Negative S are found for $x < 0$, positive S for $x > 0$.

the plasma center has to be constant and independent of R. When measured along the x-axis, see figure 1, the flux density is decreasing with increasing $|x|$ as found experimentally [20]. The distribution of flux density along the poloidal angle in the x–y-plane need not be constant since the symmetry is broken by the plasma ∇B-drift in the y-direction.

Previous studies [18, 20] demonstrated that significant parts of the turbulent plasma losses in the Blaamann device were due to coherent structures in the form of 'streamers' associated with relatively narrow flux-channels stretching through a part of the plasma predominantly in the radial direction. The features are reminiscent of related observations in linear devices [23]. Plasma transport by 'blobs' has been discussed in the literature [5, 24–30]. The randomly varying flux signal is for such cases composed of a distribution of coherent structures rather than being the result of a random walk process. It will be argued that signals obtained by distributing coherent structures in a data record also give rise to some universal features relating the skewness and kurtosis of the flux signal by a simple algebraic form.

2.2. Experimental skewness–kurtosis relations

Using data from Blaamann we can make a scatter diagram of the skewness S and the kurtosis K of the signal, and make a fit to the form of (1). Results are shown in figure 6 with filled black circles, together with a solid line for the best parabolic fit.

The distribution of the $(S,\ K)$-values forms a relatively compact cluster for $x > 0$, while we for $x < 0$ find a distribution along a parabolic fit which is here $K \approx 1.7S^2 + 6.8$ for a helium plasma. We will later argue that the density of flux structures in the time records is the same at all positions x. The forms and amplitudes of the bursts are, however, varying with x, but seemingly in such a way that $(S,\ K)$ retains a robust parabolic relation.

The large filled circular symbols in figure 6 refer to experiments in helium gas. We also have data for similar

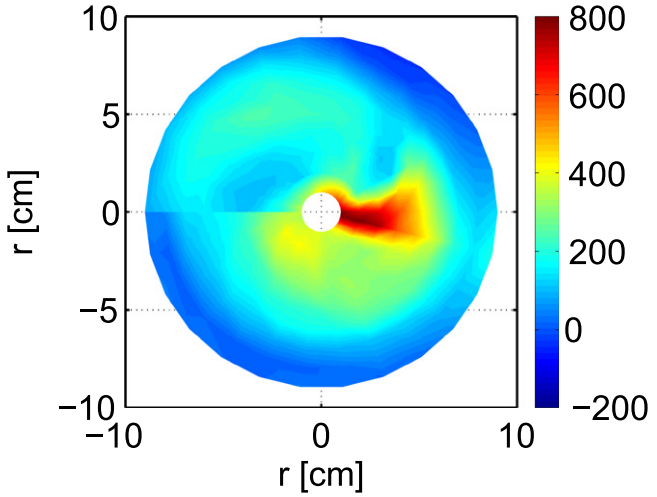

Figure 7. Experimentally obtained estimate of a coherent plasma burst. The color code is in arbitrary units. The result is obtained by conditional averaging [20], assuming a frozen turbulence model where the burst is moving in the azimuthal direction with little change in shape within the time it takes to move its own width. The imposed condition is $d\phi/dt < -1.5\ \sigma_R$ in terms of the root mean square (rms) value, σ_R, of the time derivative of the reference probe signal, see figure 1. A supplementary condition was that the flux was in the positive x-direction. The structure spans most of the shear-free rotational part of the plasma column. The shape of the structure varies with radial position.

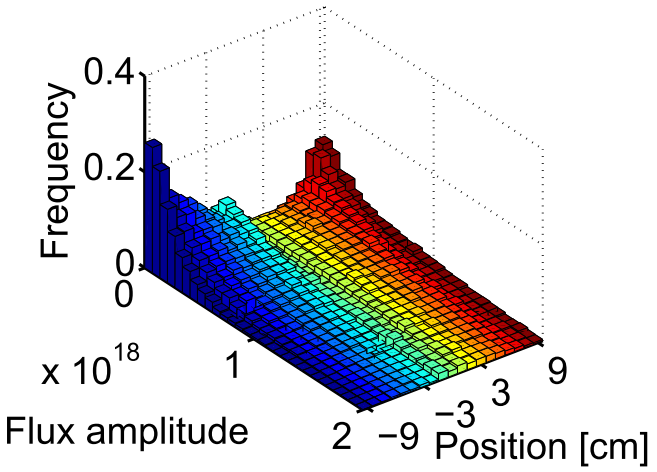

Figure 8. Distribution of the amplitude of the local maxima in the flux signal for different x-positions of the movable probe. Flux units are $s^{-1}\,m^{-2}$. The polarity of the flux signal $\Gamma(t)$ is changed for $x < 0$ so that all maxima correspond to a radially outgoing plasma flux for both $x > 0$ and $x < 0$. The color coding refers to the spatial positions x. Note the asymmetry in the distributions for $x > 0$ and $x < 0$.

experiments in argon (small dots). Data for several different experimental conditions (two neutral pressures and different values of the toroidal field, 16 combinations all-together) are available. For the helium data we have typically five records for each of the 19 spatial positions shown in figure 1, but only one per x-position for the experiments in argon. The statistical uncertainty in the latter data is therefore more than doubled, explaining at least partly the larger scatter. Here the scatter is too large to allow a meaningful analytical parabolic fit but by visual inspection we can observe a parabolic boundary. The shift in the best parabolic fit is however significant and larger than the average scatter in the data.

2.3. Coherent structures

A detailed analysis of the data (see sample in figure 3) indicated that the plasma flux was dominated by large coherent structures, or bursts of plasma propagating in the radial direction. The bursts had mostly positive polarity (corresponding to outwards plasma flux) but also negative bursts could be found. In order to substantiate the interpretation in terms of coherent structures we carried out a conditional analysis [31, 32] using the floating potential of the fixed reference probe marked by an open circle in figure 1, and making a standard conditional analysis of the fluctuating signals. An example illustrating the spatial variation of a coherent plasma burst detected in the flux signal $\Gamma(\mathbf{r}, t)$ at a fixed time is shown in figure 7. The result is obtained by conditional averaging [31] of the flux signal for positive x-positions and then 'translating' a temporal variation to angular positions with the known rotation velocity of the plasma column. In the central part of the plasma cross section (for $|x| < 6$ cm), we have evidence of a solid-body rotation of the plasma, and the structure seems to retain a coherent shape in this region, to be deformed by the rotational shear close to the plasma edge.

The result shown in figure 7 demonstrates that the plasma transport can be due to structures spanning most of the radial part of the plasma column. An alternative possibility could be transport due to small structures distributed over $0 < r < R$, moving plasma in several steps eventually to be lost to the walls of the confining vessel. We found no evidence in support of this latter model in our experiment. The results in figure 7 are supported by a 'conditional reproducibility' analysis [32] (derived from a conditional variance [33]) demonstrating that the observed burst is associated with a well defined spatial form, and it is therefore justified to call it a 'structure'.

The result in figure 7 illustrates that the observed structure crosses the entire plasma column in the radial direction: if it is detected at one x-position with $x > 0$ it will be detected in all. Consequently, the density of such pulses will be the same in all records as assumed in section 2.2, but the width and shape of the structures depend on x.

2.4. Flux maxima distributions

The pulse amplitude distribution $P_a(a)$ also contains important information. We estimated the amplitude distribution of the local maxima experimentally, with results given in figure 8. Extremum distributions require specially long records to give a good resolution of $P_a(a)$ since only a fraction of the data correspond to maxima or minima. We note that in our case small amplitudes are the most probable, indicative of the random noise level. For larger amplitudes we find the

probability density of local maxima to decrease approximately exponentially. The number of small amplitudes is particularly large at the edges of the plasma, where the smallest amplitudes are also the most probable ones. This is the region where the signatures of the coherent structure in figure 7 are deteriorating. At smaller radial distances, the local amplitude distribution has its maximum at some finite value. We have no *a priori* reason to expect that these features are universal, but the results demonstrate that relevant amplitude distributions can be estimated experimentally. The information will be relevant for a subsequent modeling.

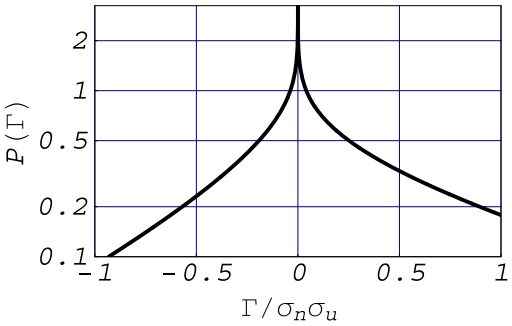

Figure 9. The probability density (2) in logarithmic presentation obtained for $\rho = 0.35$. This value of the correlation brings results from (2) close to those found in the Blaamann torus [20], and also in qualitative agreement with the first measurements of probability densities of turbulent fluxes [3].

3. Skewness–kurtosis relations

A basic result from the analysis of the present study is that the dominant plasma losses in the Blaamann torus are due to coherent bursts emerging from the plasma column [2, 17, 32]. As discussed in the following, a signal constituted of such coherent entities has certain general properties, manifested for instance by relations between various moments of probability distributions. Rather than modeling probability densities [16], we consider the physical processes in terms of the observed structures. An alternative and simpler analysis can be based on a model assuming correlated Gaussian density $\tilde{n}$ and velocity $\tilde{u}$ fluctuations. This model is outlined first. In many ways it can account for several of the observed features, but it turns out to be too restrictive by predicting all such processes to be described by the same relation between skewness and kurtosis, the only free parameter being the correlation coefficient ρ. More general models can be constructed based on randomly distributed structures in the flux signal. The additional parameters entering here will account for the shape of these structures.

3.1. A reference model based on correlated Gaussian density and velocity fluctuations

A reference model for the plasma flux found in the literature [21] is derived from a joint Gaussian PDF for the fluctuating velocity and plasma density as

$$P\left(\tilde{n},\,\tilde{u}\right) = \frac{1}{2\pi}\frac{1}{\sigma_n\sigma_u\sqrt{1-\rho^2}} \times \exp\left(-\frac{1}{2\left(1-\rho^2\right)}\left(\frac{\tilde{n}^2}{\sigma_n^2}+\frac{\tilde{u}^2}{\sigma_u^2}-2\rho\frac{\tilde{n}\tilde{u}}{\sigma_n\sigma_u}\right)\right),$$

where $\tilde{u} \equiv \widetilde{E}_y(t)/B$ and ρ is the relevant correlation coefficient, with values $|\rho| \leqslant 1$. Two opposing quadrants in the $(\tilde{u},\,\tilde{n})$-plane give rise to transport out of the plasma, the two other quadrants give transport into the main plasma column. Introducing new variables $\Gamma \equiv \tilde{n}\tilde{u}$ and $\gamma \equiv \tilde{n}$ with the Jacobi determinant being $|\tilde{\gamma}|$, a plasma flux PDF is readily obtained [21, 34] by integration over all γ to give

$$P(\Gamma) = \frac{1}{\pi}\frac{1}{\sigma_n\sigma_u\sqrt{1-\rho^2}} \times K_0\left(\frac{|\Gamma|}{\sigma_n\sigma_u\left(1-\rho^2\right)}\right)\exp\left(\frac{\rho\,\Gamma}{\sigma_n\sigma_u\left(1-\rho^2\right)}\right). \quad (2)$$

Here K_0 is the modified Bessel function of the second kind, with an integrable singularity at the origin, ensuring that $P(\Gamma)$ is integrable over ρ. The result is illustrated in figure 9. We note that Γ in addition to a fluctuating part also contains an average component

$$\langle\Gamma\rangle \equiv \int_{-\infty}^{\infty}\Gamma\,P(\Gamma)\mathrm{d}\Gamma = \sigma_n\sigma_u\rho,$$

with the variance

$$\sigma_\Gamma^2 \equiv \int_{-\infty}^{\infty}(\Gamma-\langle\Gamma\rangle)^2P(\Gamma)\mathrm{d}\Gamma = (\sigma_n\sigma_u)^2\left(1+\rho^2\right).$$

The marginal processes for $\tilde{u}$ and $\tilde{n}$ are Gaussians, but the flux process $\Gamma = \tilde{n}\tilde{u}$ is not.

The analytical expression [21] shown in figure 9 resembles the experimental results from Blaamann shown in figure 5. We can, however, not take a seeming agreement between the experimentally observed flux-PDF and (2) as an indication of the underlying correlated Gaussian model to be correct or at least being a good approximation.

The marginal PDFs for density $P(\tilde{n})$ and velocity $P(\tilde{u})$ from the Blaamann experiment can be approximated by Gaussian distributions, although within some error [20]. The joint PDFs shown in figure 4 have no symmetry line in the $(\tilde{n},\,\tilde{u})$-plane, and are thus not well approximated by products of correlated Gaussian distributions. Consequently we can at best expect the skewness–kurtosis relation obtained by (2) to be an approximation, or rather a guide.

The probability density (2) has skewness $S = 2\rho\,(3+\rho^2)/(1+\rho^2)^{3/2}$ and kurtosis $K = 3(3+14\rho^2+3\rho^4)/(1+\rho^2)^2$, which in a parametric plot (with ρ being the parameter) is found to have a near parabolic form, well approximated (within 2–3%) by $K = (3/4)S^2 + 9$, with the restricted ranges $|S| \leqslant 2\sqrt{2}$ and $9 \leqslant K \leqslant 15$. Both S and K are independent of σ_n and σ_u. The sign of ρ determines the

sign of the average flux as well as the skewness of the flux-PDF. For an idealized experiment with a magnetized plasma column following (2) we might have σ_n and σ_u as well as the correlation ρ varying with radial position, but the skewness and kurtosis obtained at any position will be somewhere on the curve determined by $(S(\rho), K(\rho))$. The model (2) is thus restrictive by assigning the constants in $K = AS^2 + C$ fixed values $A \approx 0.75$ and $B \approx 9$ for *any* experiment. This is found to be unduly restrictive for practical applications in describing experimental results. In order to accommodate also data from the Blaamann experiment as shown in figure 6, the model has to be modified.

Noting the presence of coherent flux structures as in figures 3 and 7, we propose models using a superposition of flux bursts. The models give a better and more general basis for modeling turbulent transport. We find that the skewness–kurtosis relation associated with the flux-PDFs serve as a useful basis for distinguishing models.

Our analysis addresses the plasma flux signal, but the arguments are readily applicable also for a density signal, as discussed by other authors [4, 6].

3.2. Simple model based on coherent structures

In order to discuss the possibility for a systematic relationship between skewness and kurtosis of the plasma flux signal we propose first a simple two-level model, that accounts for the observed presence of coherent structures. We assume that the flux is 'burst-like', i.e. it is either vanishing or it assumes a constant positive value $\gamma > 0$ in a short time interval $\Delta\tau$. The time variation of the flux event thus has a so called 'top hat' shape. The random process is assumed to be time stationary, and the probability α with $0 \leqslant \alpha \leqslant 1$ for encountering a plasma burst at some given position is independent of time. It is essential for the following discussion that flux events do not overlap: in this sense the present approach differs from others [6].

The probability density for the plasma flux in this basic model is

$$P(\Gamma) = (1 - \alpha)\delta(\Gamma) + \alpha\delta(\Gamma - \gamma), \tag{3}$$

where the first term accounts for the cases where the flux vanishes, i.e. at times where no plasma burst is intercepted at the selected position. We readily obtain $\langle\Gamma^m\rangle = \alpha\gamma^m$ with $m = 1, 2, 3, \ldots$, giving average value $\langle\Gamma\rangle = \alpha\gamma$, variance $\sigma^2 \equiv \langle(\Gamma - \langle\Gamma\rangle)^2\rangle = \alpha(1 - \alpha)\gamma^2$, skewness $S = \alpha(1 - 3\alpha + 2\alpha^2)\gamma^3/\sigma^3$ and kurtosis $K = \alpha(1 - 4\alpha + 6\alpha^2 - 3\alpha^3)\gamma^4/\sigma^4$, implying the exact relation $K = S^2 + 1$ for all α. Generally it can be shown that $K \geqslant S^2 + 1$ holds for any probability distribution [35], with the exception of PDF's with $\sigma = 0$, which are singular in the present context. The simple analytical model (3) and its generalizations have been widely discussed in, for instance, studies of concentration fluctuations in turbulent environments [9–14].

For the simple two-level model discussed here it is not essential that all structures have the same duration [9, 36, 37], thus we can have $\Delta\tau$ to be statistically distributed.

For a long time record of duration $\mathcal{T}$, we have $\alpha = \mu\Delta\tau$ where $\mu \approx \langle N\rangle/\mathcal{T}$ is the number density of the appropriate flux-pulses in the record. Uncertainties due to end-effects in the time record, can be made arbitrarily small by increasing $\mathcal{T}$. When μ is small, the distribution of the number N of pulses in a record can be approximated by a Poisson distribution, $P(N) = (\mu\mathcal{T})^N \exp(-\mu\mathcal{T})/N!$. More general distributions can be introduced where a minimum burst separation is ensured, i.e., a form where the positions of successive pulses are related as $x_{j+1} = x_j + \Delta\tau + X$, where $X > 0$ can be randomly distributed [38, 39]. The number of pulses or structures in any given record can not exceed $N_m \equiv \mathcal{T}/\Delta\tau$, and it can not be argued that a limiting case exists with $\mu \to \infty$, resulting in a Gaussian probability density. In the process proposed by, for instance, Campbell [40, 41], structures are allowed to overlap and a Gaussian process results by the central limit theorem [38, 39] when the number of overlapping structures increases on average as $\mu \to \infty$. The Gaussian limit is not reached for large structure densities with models like ours where structures do not overlap. The present model is thus inherently non-Gaussian for any α.

3.3. Model with statistically distributed pulse amplitudes

The model (3) can be generalized by allowing for burst events containing a random amplitude parameter a with probability density $P_a(a)$. In principle the amplitude can assume both signs even though the average is different from zero. Taking a as an amplitude factor we omit cases where the shape of the structure can depend on its magnitude, but the analysis can be extended to include also such cases. With a finite temporal duration $\Delta\tau$ of the flux event we here exclude Gaussian or exponential pulses which in principle extend from $-\infty$ to ∞. In the appendix we outline a derivation that relaxes this restriction.

We denote the pulse form by $G_a(\tau)$ for $0 \leqslant \tau \leqslant \Delta\tau$ and $G_a(\tau) = 0$ otherwise, and take $\Delta\tau$ to be the same for all pulses, irrespective of a. One example could be $G_a(\tau) = a\sin^p(\pi\tau/\Delta\tau)$ for $0 \leqslant \tau \leqslant \Delta\tau$, where p is a deterministic fitting parameter. With this generalization we find the flux probability density to be

$$P(\Gamma) = (1 - \alpha)\delta(\Gamma) + \frac{\alpha}{\Delta\tau}\int_{-\infty}^{\infty}\int_{0}^{\Delta\tau}\delta\big(\Gamma - G_a(\tau)\big)\mathrm{d}\tau P_a(a)\mathrm{d}a. \tag{4}$$

For the 'top hat' pulses assumed in e.g. (3) the amplitude probability density will be the same as $P_a(a)$, but in general the two PDFs are different.

The previous results for $\langle\Gamma\rangle$, σ^2, S and K are now readily generalized [14, 36]. We find, for instance

$$\langle\Gamma^m\rangle = \frac{\alpha}{\Delta\tau}\int_{-\infty}^{\infty}\int_{0}^{\Delta\tau}G_a^m(\tau)\mathrm{d}\tau P_a(a)\mathrm{d}a. \tag{5}$$

For completeness, we might add that (except for the top hat signal) the distribution of amplitudes $P_a(a)$ is not simply related to the probability density of the signal amplitude.

Within the present model, a temporal signal will be composed of pulses with shape $G_a(\tau)$ placed at random positions (without overlap) and with randomly distributed amplitudes. The ensemble average will give the basic statistical averages, the skewness and kurtosis in particular, with values depending on the parameters used. As demonstrated by examples in the following, the values of skewness and kurtosis will satisfy approximate parabolic relations for varying parameters for a wide range of pulse shapes and basic statistical distributions.

Given the parameters and distributions entering the expression (4), the skewness and kurtosis of the turbulent plasma fluxes are uniquely determined. *If* a universal relation between S and K is postulated (as found in the literature describing fluctuations in, for instance, plasma density [4, 6]), this implies universal properties of $G_a(\tau)$. To illustrate such a possible universal relation we again consider the example $G_a(\tau) = a\,\sin^p(\pi\tau/\Delta\tau)$ for $0 \leqslant \tau \leqslant \Delta\tau$. Using (4) we then obtain the skewness and kurtosis $S = S(\alpha)$ and $K = K(\alpha)$, where the probability α now enters as a parameter. A parametric plot of K versus S for varying α is shown in figure 10(a) for various choices of p but constant amplitudes a, i.e., $P_a(a) = \delta(a - 1)$. We have analytical expressions for the curves shown, but the expressions are too long to be included here. We note that $p > 2$ will have $S > 0$ for all α with the present model. In particular for $p = 2$ we have $S \to 0$ for $\alpha \to 1$. In general for basic pulses $G_a(\tau)$ having positive polarity as in our case, small values of α will give positive skewness, while possibly negative values are found for large α as understood by basic arguments [14]. The limit of small α is the relevant one for the present application. A parabolic relation in the form (1) will appear as a good fit in all of the cases shown, although the basic pulse shape is different from case to case, see figure 10(b). One conclusion from this analysis is that the skewness–kurtosis relation is only weakly dependent on the 'spikiness' of the basic structures. The raw data in figure 3 indicates that $p > 4$ will give the best models for the spiky basic structures observed, but this parameter is only of minor importance for the resulting S–K relation. The conspicuous consequence of 'spiky' basic structures entering the time series is a restriction on the skewness range, allowing only positive values (for positive pulse polarities, negative skewness for negative polarities) for large values of the parameter p.

Additional information, supplementing what is found in figure 10, is given in figure 11. Here we present the variation of the skewness and the kurtosis for varying parameter $0 \leqslant \alpha \leqslant 1$. The line coding is the same as in figure 10 to facilitate comparison. As the exponent parameter p in $G_a(\tau)$ given before is changed, we note that the negative range of S is changed as well, and for instance for $p = 4$ (red curve) we have $S > 0$ for all α.

In the discussion before we implied that a positive structure gives transport out of the plasma column. This will be the case for $x > 0$. For the high magnetic field side ($x < 0$ in figure 1) we have negative structures giving net transport out of the plasma.

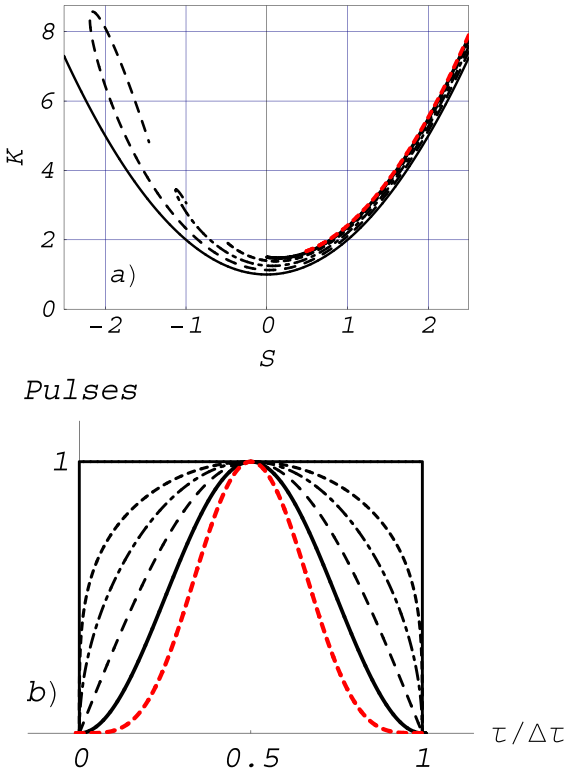

Figure 10. A parametric presentation of skewness versus kurtosis $(S(\alpha), K(\alpha))$ with varying α for selected model signals is shown in (a). The heavy solid line gives the 'top hat' model for reference, where $K = S^2 + 1$, while the first dashed line has $G(\tau) = \sin^p(\pi\tau/\Delta\tau)$ with $p = 1/4$, the next dashed–dotted line $p = 1/2$, the next dashed line has $p = 1$, the next solid line $p = 2$. A dashed red line for $p = 4$ will be almost indistinguishable from this, but it starts for a slightly larger S-value. We have taken all pulse amplitudes a to be equal. In (b) we show the temporal variation of the basic pulses entering the construction of (a). We show the 'top hat' form (which corresponds to $p = 0$), and $G(\tau) = \sin^p(\pi\tau/\Delta\tau)$ with $p = \frac{1}{4}, \frac{1}{2}$, 1, 2 and $p = 4$.

To illustrate the effect of a distribution in pulse amplitudes a, we show in figure 12(a) the case where all pulses have the same form, here $G(\tau) = a\,\sin(\pi\tau/\Delta\tau)$, but where the amplitude distribution $P_a(a)$ is a Gaussian is illustrated in figure 12. The results are representative also for other distributions. The particular case where $P_a(a) = \delta(a - 1)$ is found in figure 10. The general observation is that the relation between kurtosis and skewness of the form $K = AS^2 + C$ remains a good approximation in a restricted range, but the numerical values of A and C depend on the width of $P_a(a)$. We note also that we can have a linear component DS (see for instance the first curve above the $K = S^2 + 1$ reference in figure 12) as mentioned in the Introduction, but the numerical value of D is usually small.

The wider the pulse amplitude distribution, the larger is the deviation from the reference 'top hat' case with $K = S^2 + 1$. A wide amplitude distribution also reduces the range of variability of S. Note that the PDF used in this model (see figure 12(b)) allows also for small inward plasma bursts

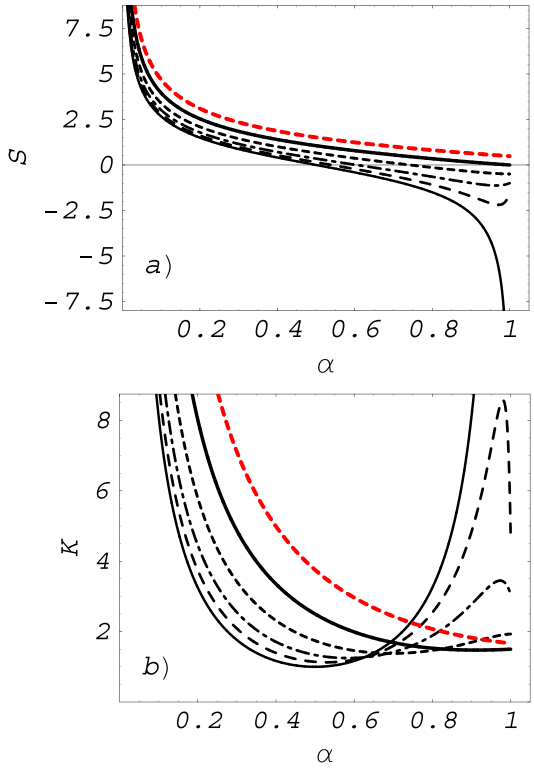

Figure 11. A parametric presentation of the skewness in (a) and the kurtosis in (b) for varying α. Line symbols and color are as in figure 10.

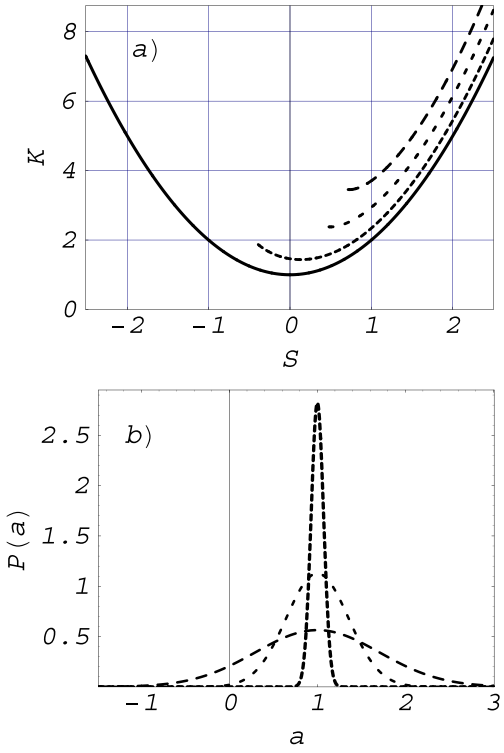

Figure 12. Modifications in figure 10(a) for the case where the amplitudes a have a statistical distribution as shown in (b). In general we find that the wider the distribution $P_a(a)$, the larger is the deviation from the reference case (shown with solid line) where $K = S^2 + 1$. In this figure we use a form $G_a(\tau) = a\,\sin(\pi\tau/\Delta\tau)$.

(as in the raw data in figure 3), i.e., the probability density extends to negative a. If we, with a fixed distribution $P_a(a)$, repeat the analysis in figure 12 with $G_a(\tau) = a\,\sin^p(\pi\tau/\Delta\tau)$ taking $p < 1$, we find that the curves approach the line $K = S^2 + 1$ for decreasing p. The general trend is that a point $(S(\alpha), K(\alpha))$ for a fixed value for α moves towards larger positive values of S and increasing K when the parameter p is increased. 'Spiky' shapes for $G_a(\tau)$, i.e., increasing p-exponents, tend to give larger kurtosis. Distributed pulse amplitudes (as in figure 12) tend to give more positive skewness and increasing kurtosis for fixed pulse-shapes and fixed α when the amplitude distribution becomes wider. The width of the amplitude probability density has, however, a stronger influence on the skewness–kurtosis relation than the spikiness of the basic pulse model.

There is no universal form for the amplitude distribution $P_a(a)$, except for the case of Gaussian random noise. As we illustrated in figure 8 by an example from the Blaamann torus, it is feasible to obtain experimental estimates for $P_a(a)$ at least for large a. Gumbel probability densities are being associated with the statistics of the maxima of a random variable [42, 43]. A closer analysis of the possible relevance of this class of distribution for our data represents a future study.

As an illustration we show in figure 13 four cases with double-sided exponential distributions. The larges S-values are found for the most asymmetric $P_a(a)$-distribution, while the K-variation changes comparatively little. The parameter p that determines how 'spiky' the individual pulses are, seems to have modest importance, it merely restricts the range of S–K variations, spiky structures restricting the lower K-range in figure 13. It is thus possible to obtain analytical results which come close to those found experimentally, see figure 6. We expect that the missing contributions for small skewness are caused by the poor fit to the observed probability density at small values of the maxima in figure 8. In this range the double-sided asymmetric exponential distribution is no longer adequate.

Our analysis so far emphasized empirical relations between skewness and kurtosis of data from turbulent magnetized plasmas since these have been studied most, as also reported in the literature. As a part of our analysis we also obtained expressions for the entire probability densities, as in e.g. (4). For arbitrary distributions for $P_a(a)$ and pulse shapes, only little can be said concerning the general properties of $P(\Gamma)$ but for the special shapes where a enters only as an amplitude factor we can obtain some direct analytical results. With $G_a(\tau) = aG(\tau)$ in (4) reduces to

$$P(\Gamma) = (1 - \alpha)\delta(\Gamma) + \frac{\alpha}{\Delta\tau}\int_0^{\Delta\tau} \frac{P_a\left(\frac{\Gamma}{G(\tau)}\right)}{|G(\tau)|}\mathrm{d}\tau, \qquad (6)$$

with $\Delta\tau$ representing the support of the basic structure. Since $P_a(a)$ is normalized, it must decrease faster than $1/a$ as $|a| \to \infty$. Except at $\Gamma = 0$, there are thus no singularities

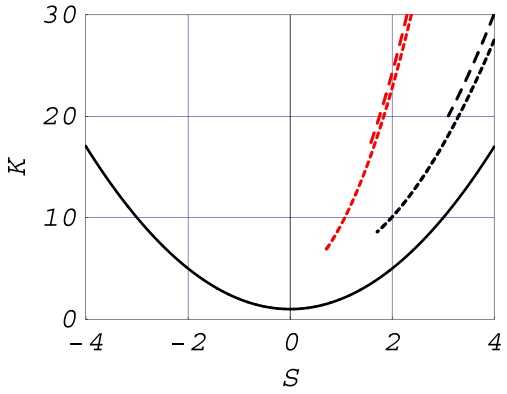

Figure 13. Illustration of the case where we use double-sided asymmetric exponential amplitude distributions, i.e. $P_a(a) = (A1 + A2)^{-1} \exp(a/A1)$ for $a < 0$ and $P_a(a) = (A1 + A2)^{-1} \exp(-a/A2)$ for $a > 0$. We show the top hat reference with full line and curves for $(A1, A2) = (0.275, 0.1)$ with black lines, and $(A1, A2) = (0.275, 0.2)$ with red lines, both with $p = 1/4$ and 4. The scale of the figure is chosen to facilitate comparison with figure 6.

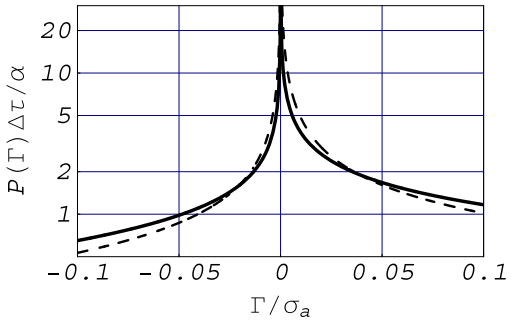

Figure 14. Flux probability densities for a signal constructed by using pulses of the form $a \sin^p(\pi\tau/\Delta\tau)$ with $p = 2$ (full line) and $p = 4$ (dashed line). The flux pulse amplitude probability density is $\exp(-(a - \langle a\rangle)^2/\sigma_a^2)/\sqrt{\pi\sigma_a^2}$, as in figure 12(b). For the two cases shown here we used $\langle a\rangle/\sigma_a = 0.35$.

associated with the limits where $G(\tau) \to 0$. Even with the present simplifying assumptions, the integral in the result (6) has to be solved numerically in most cases. Some cases can, however, be solved analytically. If we, for instance, take $G(\tau) = \sin^p(\pi\tau/\Delta\tau)$ and $p = 2$ we find (apart from the $\delta(\Gamma)$-function contribution) $P(\Gamma) = (\alpha/\Delta\tau) \exp\left(-\frac{1}{2}\Gamma^2\right) K_{\frac{1}{4}}\left(\frac{1}{2}\Gamma^2\right)\Big/(\pi\sqrt{2})$ with a singularity for $\Gamma = 0$ for the symmetric case $P_a(a) = \exp(-a^2)/\sqrt{\pi}$. We introduced the modified Bessel function of the second kind $K_{\frac{1}{4}}$. This particular solution has no net plasma flux due to the chosen symmetry. Also, some examples with finite averages have analytical solutions, but these tend to be rather lengthy. Numerically obtained results are shown in figure 14. It is interesting to note how much this PDF resembles the one shown in figure 9, although the underlying models are completely different (see also the discussion in the appendix). We find the similarity with experimentally obtained results [20] even more interesting. The analytical expression for the probability density (6) contains free parameters that can accommodate different physical conditions. These parameters influence the entire probability density and its moments, in particular also the skewness and kurtosis, whereas in (2) only one parameter, the correlation ρ, affects S and K.

By use of (5), the average plasma flux can here be determined analytically as

$$\langle\Gamma\rangle = \frac{\alpha\langle a\rangle}{\sqrt{\pi}} \frac{\int_0^\infty \tau^{(p-1)/2} \mathrm{e}^{-\tau} \mathrm{d}\tau}{\int_0^\infty \tau^{p/2} \mathrm{e}^{-\tau} \mathrm{d}\tau}. \tag{7}$$

Note that this result is independent of the actual form of the pulse amplitude probability density $P_a(a)$: all that is assumed is that its average value exists. We find, in particular, $\langle\Gamma\rangle = \alpha\langle a\rangle/2$ for $p = 2$ and $\langle\Gamma\rangle = 3\alpha\langle a\rangle/8$ for $p = 4$. Analytical expressions for $\langle\Gamma^m\rangle$ are also readily found.

3.4. Model with statistically distributed pulse amplitudes and widths

So far we have implicitly assumed that one $\Delta\tau$ describes all pulses. Allowing for a distribution of pulse durations we have to anticipate that α depends on $\Delta\tau$, i.e. $\alpha \to \alpha_{\Delta\tau}$ with some distribution $P(\alpha_{\Delta\tau})$. It gives a simplification to assume that a and $\Delta\tau$ are statistically independent. In general, the positions of different pulse-types are constrained by the requirement $\sum_j N_j \Delta\tau_j \leqslant \mathcal{T}$ where N_j is the number of pulses of type j in the record of duration $\mathcal{T}$. This constraint is not restrictive when $\sum_j \mu_j \Delta\tau_j \ll 1$. Using $\alpha_{\Delta\tau} = \mu_{\Delta\tau}\Delta\tau$ explicitly, the result (4) can be generalized as

$$P(\Gamma) = \left(1 - \langle\alpha_{\Delta\tau}\rangle\right)\delta(\Gamma) + \int_0^\infty \int_0^\infty \int_{-\infty}^\infty \int_0^{\Delta\tau} \mu_{\Delta\tau} \delta\left(\Gamma - G_{a,\Delta\tau}(\tau)\right) \mathrm{d}\tau P_a(a) \mathrm{d}a P\left(\mu_{\Delta\tau}, \Delta\tau\right) \mathrm{d}\mu_{\Delta\tau}\, \mathrm{d}\Delta\tau. \tag{8}$$

We need not assume $\mu_{\Delta\tau}$ and $\Delta\tau$ to be statistically independent. For a special class of models with the simple scaling property $G_{a,\Delta\tau}(\tau) = aF(\tau/\Delta\tau)$ for $0 \leqslant \tau \leqslant \Delta\tau$, we find $\langle\Gamma^m\rangle = \langle\mu_{\Delta\tau}\Delta\tau\rangle\langle a^m\rangle \int_0^1 F^m(z)\mathrm{d}z$, where we have the probability of encountering a plasma burst irrespective of its width and amplitude to be $\langle\alpha_{\Delta\tau}\rangle = \langle\mu_{\Delta\tau}\Delta\tau\rangle$. We see that the results of figure 10 apply also for these scaled pulses, since $\Delta\tau$ can be included in an effective parameter, which now becomes $\langle\alpha_{\Delta\tau}\rangle$. Generally we find that pulse shapes that have a narrow half-width in comparison to their duration $\Delta\tau$ give larger positive skewness and larger kurtosis for $P(\Gamma)$. Pulses that are narrow in this sense (for example half a period of $\sin^n t$ for some large exponent n, or a cnoidal wave) will only give positive contributions to the skewness.

A special case is where the flux signal is composed of two structures with different shapes. This could be due to non-overlapping pulses with $\{\Gamma \equiv \tilde{n}\widetilde{E}/B > 0,\ \tilde{n} > 0,\ \widetilde{E}/B > 0\}$ and $\{\Gamma \equiv \tilde{n}\widetilde{E}/B > 0, \tilde{n} < 0, \widetilde{E}/B < 0\}$, respectively. The analytical expressions for $P(\Gamma)$ are readily generalized to include this case.

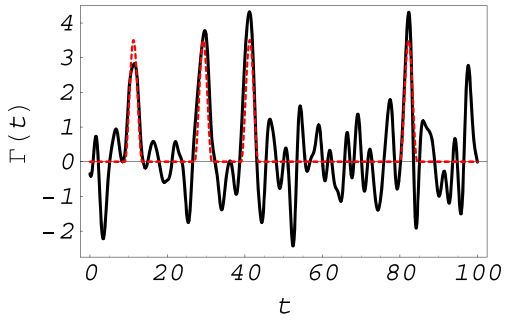

Figure 15. Illustration of a synthetic signal consisting of pulses of the form $a\ \sin^2(\pi\tau/\Delta\tau)$ with additive Gaussian noise with zero mean. The dashed red line gives the contribution of the structures alone, the black line includes the additive noise. We kept all pulse amplitudes and widths to be the same, ($a = 3.5$, $\Delta = 4.5$) in order illustrate how the added noise gives a distribution in the local maxima. Note that the noise itself contains sporadic large pulses.

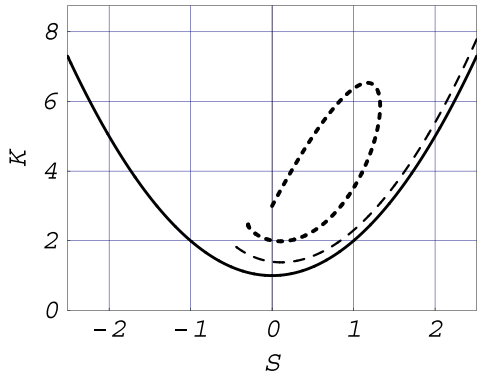

Figure 16. Illustration of the effects of additive Gaussian noise. The solid line gives the reference curve $K = S^2 + 1$, the thin dashed line is the result without noise as in figure 10, and the heavy dotted line shows results for a constant noise level with $\sigma = 0.2$. We use the pulse-form $G_a(\tau) = a\ \sin(\pi\tau/\Delta\tau)$ for $0 \leqslant \tau \leqslant \Delta\tau$ and fixed amplitude a. The variation along the curves is also here due to a varying probability α defined in the discussion of, for instance, (3). For $\alpha \ll 1$ the structures are rare, and the signal is dominated by the Gaussian noise giving $(S, K) \approx (0, 3)$.

3.5. Model with additive noise

Even with the generalizations given before, the present model is so far over-idealized in one respect by including only bursty events. To make the model even more realistic, we assume some independent additive random plasma flux fluctuations Γ_2, implying $\Gamma = \Gamma_1 + \Gamma_2$, where Γ_1 is associated solely with the burst events discussed before, while Γ_2 accounts for the added noise. Studies of synthetic data with additive noise have been reported [7] and the consequences for a skewness–kurtosis relation were illustrated as well.

Within our model we can give an illustrative analytical result by considering the special case where the additive random plasma flux contribution has a zero mean Gaussian PDF with a variance σ_r^2, implying that this part of the signal propagates plasma in and out of the plasma column with equal probability. An illustrative sample of such synthetic data is shown in figure 15 to be compared with the top trace in figure 3. A random distribution of pulse amplitudes will make the similarity even more conspicuous. Note that the noise itself contains sporadic large pulses that can be mistaken for structures [44]. The average $\langle\Gamma\rangle$ remains the same as for (8) also for additive random noise with zero mean, while the variance becomes $\sigma^2 \equiv \langle\Gamma^2\rangle - \langle\Gamma\rangle^2 = \langle\Gamma_1^2\rangle - \langle\Gamma_1\rangle^2 + \sigma_r^2$, where the two first terms are obtained from (8). The third moment remains unchanged $\langle(\Gamma - \langle\Gamma\rangle)^3\rangle = \langle\Gamma_1^3\rangle + 2\langle\Gamma_1\rangle^3 - 3\langle\Gamma_1^2\rangle\langle\Gamma_1\rangle$, but the normalization by $\sigma^{3/2}$ that is entering the skewness is changed. For the fourth moment we find

$$\begin{aligned}\langle(\Gamma - \langle\Gamma\rangle)^4\rangle &= \left\langle\Gamma^4\right\rangle - 3\langle\Gamma\rangle^4 + 6\left\langle\Gamma^2\right\rangle\langle\Gamma\rangle^2 - 4\left\langle\Gamma^3\right\rangle\langle\Gamma\rangle \\ &= \left\langle\Gamma_1^4\right\rangle - 3\left\langle\Gamma_1\right\rangle^4 + 6\left\langle\Gamma_1^2\right\rangle\left\langle\Gamma_1\right\rangle^2 \\ &\quad - 4\left\langle\Gamma_1^3\right\rangle\left\langle\Gamma_1\right\rangle \\ &\quad + 6\sigma_r^2\left(\left\langle\Gamma_1^2\right\rangle - \left\langle\Gamma_1\right\rangle^2\right) + 3\sigma_r^4. \end{aligned} \tag{9}$$

We used that $\langle\Gamma_2^4\rangle = 3\sigma_r^4$ for a Gaussian random process. With these generalizations we believe that the model can describe a wide range of experimental conditions, in particular also the bursty plasma transport observed in Blaamann and similar devices.

In order to illustrate the consequences of additive noise, we show in figure 16 with heavy dotted line the skewness–kurtosis relation for a case where the constant noise level has $\sigma = 0.2$. The details of the curve depend on the form chose for $G_a(\tau)$. The results in figure 16 are valid irrespective of the correlation time of the Gaussian noise in relation to the width of the pulses. In the flux probability density we find that a small level of Gaussian noise will round-off the 'cusp' at the origin found in for instance figure 14.

As the parameter $\alpha \to 0$, the noise dominates the signal and we find $K \to 3$ and $S \to 0$ for Gaussian noise with zero mean. By analyzing different parameter combinations, we find that by restricting α-values to a range where $\langle\Gamma_1\rangle \geqslant \sigma$ this part of the curve is not accessed. For a wide range of α-values we find again that a relation in the form $K = AS^2 + C$ remains applicable with properly chosen values for the constants A and C. We note that the range of variability of these constants is modest: in all the cases illustrated here we have, for instance, $1 \leqslant C < 2.1$. If we restrict the analysis to the range $-1 \leqslant S \leqslant 1$ we find similarly $1 \leqslant A \leqslant 2.5$, the largest deviations from the reference case being caused by the additive noise.

The analysis of skewness–kurtosis relations outlined in this section can be generalized to several other related problems. The entire probability density for the signal composed by structures and independent additional random noise can be obtained by a convolution of the noise PDF (usually a Gaussian with zero mean) and a PDF of the form (8).

4. Conclusions

The present study addresses observations of seemingly robust relations between skewness and kurtosis of the form

$K = AS^2 + C$ observed in a number of experiments in turbulent plasmas as well as in turbulent neutral flows. Using data from the Blaamann experiment as a reference we propose a general model for synthetic flux signals where a number of analytical results can be obtained.

Instead of radial plasma flux resulting from correlated Gaussian distributions [21, 34, 45] we suggest a model based on flux signals composed of random non-overlapping pulses characterized by some measurable parameters, distributed amplitudes for instance. Some general analytical results, such as (7) can be obtained by the model. We believe that the seemingly robust skewness–kurtosis relations can also be adequately explained by this model. The appendix contains a discussion of the relation of present results to the Rice model for synthetic signals found in the literature [38]. For given experimental conditions as in the Blaamann torus we can assume that flux structures traverse the plasma in the radial direction, see figure 7. This means that the number of large coherent structures will be the same in each of the records from the selected probe positions. The temporal duration $\Delta\tau$ of an event (i.e. as given by $G_a(\tau)$ in (4)) and its amplitude and width as sampled at some position x depends in general on the position, see figure 7. The probability α entering for instance (5) will therefore also in general depend on position. The change in numerical coefficients in the (K, S)-relation is thus caused by a change in shape of the basic flux structures as well as their statistical properties when we change the filling gas from helium to argon in the experiment.

Our analysis emphasized empirical relations between skewness and kurtosis of data from turbulent magnetized plasmas since these have been studied most, as also reported in the literature. As a part of our analysis we also obtained expressions for the entire probability densities, as in e.g. (4). Relatively few observations of plasma flux PDF are reported, but it seems plausible that our model (see figure 14) can be made to accommodate observations [3, 20, 22] with proper choice of parameters. Our results agree well with data from Blaamann, with samples shown in figure 5.

We used data from the former Blaamann torus for illustration, and expect that it can be worthwhile to analyze data from other similar devices in the same way. For our reference case, the discharge in helium, the general model based on narrow structures placed randomly in a record without overlap is capable of explaining, for instance, the sign of the skewness of the flux signal. We thus have $S > 0$ for $x > 0$ with net plasma flux out of the plasma in the positive x-direction, and $S < 0$ for $x < 0$ with net plasma flux out of the plasma in the negative x-direction. The level of kurtosis is consistent with a large scatter in peak amplitudes of structures, see for instance figure 12. The Blaamann data for helium and argon demonstrated also the need for some parameters accounting for deviation from the simple model (2).

Our analysis allows for inclusion of additive independent random noise, in particular allowing for a continuous transition to the Gaussian limit where the noise completely dominates the contribution from the coherent structures. By inclusion of such a noise level the model allows for modeling contributions from classical diffusion in addition to a dominant plasma transport originating from coherent structures in the flux-signal. Some studies [46, 47] have indicated that parabolic relations between skewness and kurtosis seem very robust, but a transition to the Gaussian limit $(S, K) = (0, 3)$ has to result by adding Gaussian noise of sufficient intensity. Our model satisfies this criterion.

Acknowledgments

The present data-sets were obtained in the Blaamann device at the University of Tromsø. The experiment has now been dismantled on the request of the Norwegian National Science Foundation. We would like to thank colleagues, students, and the technical staff for their contributions to the work on this experiment. In particular, we thank Terje Brundtland for his enthusiasm and tireless work in the construction and maintenance of the device. We thank also Bjørn Lybekk for his assistance with one of the figures. The present summary is presented for a special issue of *Physica Scripta* celebrating Professor Lennart Stenflo's 75th birthday. Although our interests have changed during the years, Lennart has remained an inspiration for us all. Most of all he continued to be a good friend.

Appendix. Analytical models for synthetic data

Synthetic data can often be useful for illustrating properties of real signals. In some sense it might be argued that the properties of a signal are completely understood if we are in a position to produce a synthetic data-set with statistical properties that are indistinguishable from the original data-set [48]. Several systematic methods can be found in the literature. Here we will refer to the Rice model [39, 49, 50] that has been used often. Elements of these ideas were presented before [40, 41, 51].

The model assumes the problem being described by pulses appearing randomly in time with some given spatial variation, i.e., a signal for potential is given by

$$\phi(\mathbf{r}, t) = \sum_{j=1}^{N} a\, \psi(\mathbf{r}, t - t_j), \tag{A.1}$$

where ψ denotes a space–time varying elementary potential pulse and the subscript j refers to the temporal position of this pulse in the record. The amplitude a is included for later convenience. We assume the temporal duration of the record to be finite, $\mathcal{T}$. We have $\int \psi(\mathbf{r}, t)\mathrm{d}\mathbf{r} = 0$ for all t by assumption. It turns out to be an important assumption that time instances t_j are random and uniformly distributed in the time-record. We have N to be the total number of such pulses in the given realization. We keep the detector position $\mathbf{r}$ as a reminder that the time-record changes when the detecting probe is moved.

From $\phi(\mathbf{r}, t)$ we can derive a record for the electric field by $\mathbf{E} = -\nabla\phi(\mathbf{r}, t)$. Similarly, we obtain a record for the

density as

$$n(\mathbf{r}, t) = \sum_{j=1}^{N} b\, \eta(\mathbf{r}, t - t_j), \tag{A.2}$$

where the relation between ψ and η is unspecified for the moment. Formally, we can consider the fluctuations in density and electrostatic potential as two correlated records.

By standard methods, we can obtain expressions for statistical averages as, e.g.

$$\left\langle \phi^2(\mathbf{r}) \right\rangle = \mu\, a^2 \int \psi^2(\mathbf{r}, t)\mathrm{d}t,$$

with μ being the density in the time record, i.e., average number of pulses per time unit. We have $\langle \phi(\mathbf{r}) \rangle = 0$ with the given assumption. Similar expressions can be obtained for $\langle n(\mathbf{r}) \rangle$ and $\langle n^2(\mathbf{r}) \rangle$. The density μ is the same for density and potential for the given model. With some algebra [49] a probability density for potential can be obtained as

$$P(\phi) = \frac{1}{2\pi} \int_{-\infty}^{\infty} \exp(-\mathrm{i}\phi u + \mu \int_{-\infty}^{\infty} \{\exp[\mathrm{i}ua\psi(t)] - 1\}\mathrm{d}t)\mathrm{d}u, \tag{A.3}$$

with a similar result for the fluctuating density and any component for the fluctuating electric field. It can be demonstrated analytically that $P(\phi)$ approaches a Gaussian distribution in the limit where $\mu \to \infty$, i.e. when many pulses overlap. In this limit we will have $\langle \phi^2(\mathbf{r}) \rangle$ diverging if a is constant, so it is an advantage to let $a \to 0$ in the transition in such a way that $a^2\mu$ remains constant. More generally, we can obtain similar results for an electric field component E_y or the fluctuating velocity component derived from it as

$$u_x = -\frac{1}{B} \sum_{j=1}^{N} a \frac{\partial \psi(\mathbf{r}, t - t_j)}{\partial y}.$$

In particular we have the joint PDF for velocity and fluctuating plasma density obtained at a fixed position as

$$P(n, u_x) = \frac{1}{(2\pi)^2} \int\int_{-\infty}^{\infty} \exp\left(-\mathrm{i}u_x v - \mathrm{i}nw\right) \times \exp\left(\mu \int_{-\infty}^{\infty} \{\exp\left[\mathrm{i}wb\, \eta(t) + \mathrm{i}va\, \psi'(t)/B\right] - 1\}\mathrm{d}t\right)\mathrm{d}v\, \mathrm{d}w, \tag{A.4}$$

here with $\psi'(t) \equiv -\partial\psi(\mathbf{r}, t)/\partial y$. To simplify the notation, we suppressed the spatial dependence of η and ψ' in the time integral. Statistical distributions in pulse amplitudes a and b are easily accounted for [49]. A distribution involving different pulse shapes when constructing the record for $n(\mathbf{r}, t)$, and similarly for $\phi(\mathbf{r}, t)$, is also possible, but the expressions become a little more complicated.

We can obtain other joint probability densities such as $P(\Gamma, \Gamma')$ with $\Gamma' \equiv \mathrm{d}\Gamma/\mathrm{d}t$ by generalizing (A.4) to describe superposition of pulse-like plasma flux events. This joint probability density will be particularly valuable for modeling excess time statistics [20, 44].

Again it can be demonstrated [49] that $P(n, u_x)$ as given by (A.4) approaches a joint Gaussian PDF when $\mu \to \infty$ in the form (2). The correlation coefficient for any μ is found analytically with the result $\langle nu_x \rangle = \mu ab \int \eta(\mathbf{r}, t)\psi'(\mathbf{r}, t)\mathrm{d}t/B$.

So far we have not discussed the relation between the basic pulses $\eta(\mathbf{r}, t)$ and $\psi(\mathbf{r}, t)$. An ideal limiting case assumes quasi-neutrality [52] and isothermally Boltzmann distributed electrons giving $\eta(\mathbf{r}, t) = n_0 \exp(e\psi(\mathbf{r}, t)/T_e)$, or in a linearized form $\tilde{\eta}(\mathbf{r}, t)/n_0 = e\tilde{\psi}(\mathbf{r}, t)/T_e$ for the small amplitude fluctuating components. For this case we have at any position $\mathbf{r}$

$$\langle \Gamma(\mathbf{r}) \rangle \equiv \langle \tilde{n}\tilde{u}_x \rangle = \frac{\mu n_0 e a^2}{2BT_e} \int \frac{\partial \tilde{\psi}^2(\mathbf{r}, t)}{\partial y}\mathrm{d}t.$$

Plasma is transported across magnetic field lines by the fluctuations, but for spatially bounded $\tilde{\psi}^2(\mathbf{r}, t)$ the spatially averaged flux-component $\int \langle \Gamma(\mathbf{r}) \rangle \mathrm{d}y$ will vanish, and this will be true for any spatial component of $n\mathbf{E} \times \mathbf{B}/B^2$. Net plasma transport results when a phase difference different from $\pi/2$ between $\tilde{n}$ and $\tilde{u}_x$ develops. This happens for instance when the electrons can no longer maintain a local Boltzmann equilibrium by flowing along magnetic field lines [53, 54]. Their motion can be inhibited by electron–ion collisions, giving in this case the resistive drift wave instability [53].

We have thus a model for synthetic data which as a limiting case reproduces (2) and thereby the results derived from it. An essential element in the present derivation is, however, that many pulses or structures overlap when $\mu \to \infty$, making the central limit theorem effective. If we assume pulses or coherent structures to be responsible for most of the plasma transport, it might be difficult to argue that two or more structures are present at the same time at the same spatial position. We will discuss the limit where overlap of structures is improbable, i.e., the limit of small μ.

To illustrate the transition to our new model (3) we assume that the density as well as velocity signals are composed by 'top hat' pulses with amplitudes n_1 and u_1, respectively, with a temporal overlap of duration $\Delta\tau$. Let the pulses have the two polarities with equal probability so that the average is vanishing. The sign of the density and velocity pulses are synchronized in the sense that corresponding pulses have the same signs of the amplitude. The flux signal is then composed of top hat structures as well with amplitudes $n_1u_1 > 0$ and duration $\Delta\tau$. For this case we can find the flux-PDF analytically with the result [39]

$$P(\Gamma) = \sum_{N=0}^{\infty} \frac{(\mu\Delta\tau)^N}{N!} \exp(-\mu\Delta\tau)\delta\left(\Gamma - Nn_1u_1\right) \tag{A.5}$$

with $N = 0, 1, 2, \ldots$. The result is obtained by the assumption implied also in e.g. (A.3) that pulses can overlap as $\mu \to \infty$. For small μ the probability for overlapping pulses becomes negligible and we can ignore all terms with $N \geqslant 2$ in (A.5), and retain only the lowest order terms in an expansion in powers of $\mu\Delta\tau$. The result is the flux probability

density

$$P(\Gamma) = (1 - \mu\Delta\tau)\delta(\Gamma) + \mu\Delta\tau\ \delta\big(\Gamma - n_1 u_1\big),$$

i.e. the form (3). The construction used here also emphasizes the importance of distinguishing synthetic data obtained by non-overlapping pulses as in (3), from the completely random distributions as in the standard Rice model used for (A.5). In the limit of $\mu\Delta\tau \to 0$ the two models become indistinguishable. For general pulse-forms (different from top hat pulses), we expect that (A.3) and (A.4) can be applied in the limit of $\mu\Delta\tau \ll 1$ for non-overlapping pulses. For this limit we thus find from (A.3)

$$P(\phi) \approx \delta(\phi) + \frac{\mu}{2\pi}\int_{-\infty}^{\infty} \exp(-\mathrm{i}\phi u) \times \int_{-\infty}^{\infty} (\exp[\mathrm{i}ua\ \psi(t)] - 1)\mathrm{d}t\ \mathrm{d}u,$$

where the second term will contain a μ-proportional $\delta(\phi)$ -contribution that comes in addition to the first δ-function. A similar but more lengthy expression can be obtained from (A.4) for $P(n, u_x)$ as

$$P(n, u_x) \approx \frac{1}{(2\pi)^2}\int\int_{-\infty}^{\infty} \exp\big(-\mathrm{i}u_x v - \mathrm{i}nw\big) \times \Bigg(1 + \mu\int_{-\infty}^{\infty}\{\exp\,[\mathrm{i}wb\ \eta(t) + \mathrm{i}va\ \psi'(t)/B] - 1\}\mathrm{d}t\Bigg)\mathrm{d}v\ \mathrm{d}w, \qquad (A.6)$$

where the unity term in the brackets contribute, with a δ-function as before.

Introducing the restricted probability of encountering a pulse as α in (3) gives a simple way of avoiding overlapping pulses. For illustration we used here only a model where the plasma flux associated with each pulse was positive, i.e., out of the plasma. Sporadic inwards flux components can be obtained by introducing also overlapping density and velocity pulses that has opposite polarity.

The derivation in this appendix relaxes the restriction of finite support of the individual structures used in e.g. section 3.3 and the following subsections.

References

[1] Liewer P C 1985 Measurements on microturbulence in tokamaks and comparison with theories of turbulence and anomalous transport *Nucl. Fusion* **25** 543–621

[2] Rypdal K, Grønvoll E, Øynes F, Fredriksen Å, Armstrong R J, Trulsen J and Pécseli H L 1994 Confinement and turbulent transport in a plasma torus with no rotational transform *Plasma Phys. Control. Fusion* **36** 1099–114

[3] Huld T, Iizuka S, Pécseli H L and Juul Rasmussen J 1988 Experimental investigation of flute-type electrostatic turbulence *Plasma Phys. Control. Fusion* **30** 1297–318

[4] Labit B, Furno I, Fasoli A, Diallo A, Müller S H, Plyushchev G, Podestà M and Poli F M 2007 Universal statistical properties of drift-interchange turbulence in TORPEX plasmas *Phys. Rev. Lett.* **98** 255002

[5] Cheng J *et al* 2010 Statistical characterization of blob turbulence across the separatrix in HL-2A tokamak *Plasma Phys. Control. Fusion* **52** 055003

[6] Garcia O E 2012 Stochastic modeling of intermittent scrape-off layer plasma fluctuations *Phys. Rev. Lett.* **108** 265001

[7] Guszejnov D, Lazányi N, Bencze A and Zoletnik S 2013 On the effect of intermittency of turbulence on the parabolic relation between skewness and kurtosis in magnetized plasmas *Phys. Plasmas* **20** 112305

[8] Yan N *et al* 2013 Statistical characterization of turbulence in the boundary plasma of EAST *Plasma Phys. Control. Fusion* **55** 115007

[9] Mole N and Clarke E D 1995 Relationships between higher moments of concentration and of dose in turbulent dispersion *Bound.—Layer Meteorol.* **73** 35–52

[10] Yee E and Chan R 1997 A simple model for the probability density function of concentration fluctuations in atmospheric plumes *Atmos. Environ.* **31** 991–1002

[11] Lewis D M and Chatwin P C 1997 A three-parameter PDF for the concentration of an atmospheric pollutant *J. Appl. Meteorol.* **36** 1064–75

[12] Krane B, Pécseli H L and Trulsen J 2003 Concentrations and concentration fluctuations in two-dimensional turbulence *Phys. Fluids* **15** 211–26

[13] Mole N, Schopflocher T P and Sullivan P J 2008 High concentrations of a passive scalar in turbulent dispersion *J. Fluid Mech.* **604** 447–74

[14] Jørgensen H E, Mikkelsen T and Pécseli H L 2010 Concentration fluctuations in smoke plumes released near the ground *Bound.—Layer Meteorol.* **137** 345–72

[15] Krommes J A 2008 The remarkable similarity between the scaling of kurtosis with squared skewness for TORPEX density fluctuations and sea-surface temperature fluctuations *Phys. Plasmas* **15** 030703

[16] Sandberg I, Benkadda S, Garbet X, Ropokis G, Hizanidis K and del Castillo-Negrete D 2009 Universal probability distribution function for bursty transport in plasma turbulence *Phys. Rev. Lett.* **103** 165001

[17] Rypdal K, Garcia O E and Paulsen J-V 1997 Anomalous cross-field current and fluctuating equilibrium of magnetized plasmas *Phys. Rev. Lett.* **79** 1857–60

[18] Fredriksen Å, Riccardi C, Cartegni L and Pécseli H 2003 Coherent structures, transport and intermittency in a magnetized plasma *Plasma Phys. Control. Fusion* **45** 721–33

[19] Fredriksen Å, Riccardi C and Magni S 2006 Effects of edge dc biasing on plasma rotation and transport in a toroidal geometry *Phys. Scr.* **T122** 11–14

[20] Fattorini L, Fredriksen Å, Pécseli H L, Riccardi C and Trulsen J K 2012 Turbulent transport in a toroidal magnetized plasma *Plasma Phys. Control. Fusion* **54** 085017

[21] Carreras B A, Hidalgo C, Sánchez E, Pedrosa M A, Balbín R, Garcia-Cortés I, van Milligen B, Newman D E and Lynch V E 1996 Fluctuation-induced flux at the plasma edge in toroidal devices *Phys. Plasmas* **3** 2664–72

[22] Huld T, Nielsen A H, Pécseli H L and Juul Rasmussen J 1991 Coherent structures in two-dimensional turbulence *Phys. Fluids* B **3** 1609–25

[23] Yamada T *et al* 2008 Anatomy of plasma turbulence *Nat. Phys.* **4** 721–5

[24] Garcia O E, Naulin V, Nielsen A H and Juul Rasmussen J 2005 Turbulence and intermittent transport at the boundary of magnetized plasmas *Phys. Plasmas* **12** 062309

[25] Grulke O, Terry J L, LaBombard B and Zweben S J 2005 Radially propagating fluctuation structures in the scrape-off layer of alcator C-mod *Phys. Plasmas* **13** 012306

[26] Furno I *et al* 2008 Mechanism for blob generation in the TORPEX toroidal plasmaa *Phys. Plasmas* **15** 055903

[27] Furno I *et al* 2008 Experimental observation of the blob-generation mechanism from interchange waves in a plasma *Phys. Rev. Lett.* **100** 055004

[28] Müller S H, Theiler C, Fasoli A, Furno I, Labit B, Tynan G R, Xu M, Yan Z and Yu J H 2009 Studies of blob formation, propagation and transport mechanisms in basic experimental plasmas (TORPEX and CSDX) *Plasma Phys. Control. Fusion* **51** 055020

[29] D'Ippolito D A, Myra J R and Zweben S J 2011 Convective transport by intermittent blob-filaments: comparison of theory and experiment *Phys. Plasmas* **18** 060501

[30] Labit B, Theiler C, Fasoli A, Furno I and Ricci P 2011 Blob-induced toroidal momentum transport in simple magnetized plasmas *Phys. Plasmas* **18** 032308

[31] Johnsen H, Pécseli H L and Trulsen J 1987 Conditional eddies in plasma turbulence *Phys. Fluids* **30** 2239–54

[32] Øynes F J, Olsen O-M, Pécseli H L, Fredriksen Å and Rypdal K 1998 Experimental study of low-frequency electrostatic fluctuations in a magnetized toroidal plasma *Phys. Rev.* E **57** 2242–55

[33] Nielsen A H, Pécseli H L and Juul Rasmussen J 1996 Turbulent transport in low-β plasmas *Phys. Plasmas* **3** 1530–44

[34] Papoulis A 1991 *Probability Random Variables and Stochastic Processes* 3rd edn (New York: McGraw-Hill)

[35] Wilkins J E 1944 A note on skewness and kurtosis *Ann. Math. Stat.* **15** 333–5

[36] Sawford B L and Sullivan P J 1995 A simple representation of a developing contaminant concentration field *J. Fluid Mech.* **289** 141–57

[37] Schopflocher T P and Sullivan P J 2005 The relationship between skewness and kurtosis of a diffusing scalar *Bound. —Layer Meteorol.* **115** 341–58

[38] Rice S O 1945 Mathematical analysis of random noise: II *Bell Syst. Tech. J.* **24** 46–156
reprinted by Wax N 1954 *Selected Papers on Noise and Stochastic Processes* (New York: Dover)

[39] Pécseli H L 2000 *Fluctuations in Physical Systems* (Cambridge: Cambridge University Press)

[40] Campbell N R 1909 The study of discontinuous phenomena *Proc. Camb. Phil. Soc.* **15** 117–36

[41] Campbell N R 1909 Discontinuities in light emission *Proc. Camb. Phil. Soc.* **15** 310–28

[42] Kristensen L, Casanova M, Courtney M S and Troen I 1991 In search of a gust definition *Bound.—Layer Meteorol.* **55** 91–107

[43] van Milligen B P, Sánchez R, Carreras B A, Lynch V E, LaBombard B, Pedrosa M A, Hidalgo C, Gonçalves B, Balbín R The W7-AS Team 2005 Additional evidence for the universality of the probability distribution of turbulent fluctuations and fluxes in the scrape-off layer region of fusion plasmas *Phys. Plasmas* **12** 052507

[44] Sato H, Pécseli H L and Trulsen J 2012 Fluctuations in the direction of propagation of intermittent low frequency ionospheric waves *J. Geophys. Res.* **117** A03329

[45] Naulin V, Garcia O E, Nielsen A H and Juul Rasmussen J 2004 Statistical properties of transport in plasma turbulence *Phys. Lett.* A **321** 355–65

[46] Sattin F, Agostini M, Cavazzana R, Serianni G, Scarin P and Vianello N 2009 About the parabolic relation existing between the skewness and the kurtosis in time series of experimental data *Phys. Scr.* **79** 045006

[47] Cristelli M, Zaccaria A and Pietronero L 2012 Universal relation between skewness and kurtosis in complex dynamics *Phys. Rev.* E **85** 066108

[48] Kofoed-Hansen O, Pécseli H L and Trulsen J 1989 Coherent structures in numerically simulated plasma turbulence *Phys. Scr.* **40** 280–94

[49] Rice S O 1944 Mathematical analysis of random noise: I *Bell Syst. Tech. J.* **23** 282–332
reprinted by Wax N 1954 *Selected Papers on Noise and Stochastic Processes* (New York: Dover)

[50] Pécseli H L and Trulsen J 1993 On the interpretation of experimental methods for investigating nonlinear wave phenomena *Plasma Phys. Control. Fusion* **35** 1701–15

[51] Rowland E N 1936 The theory of the mean square variation of a function formed by adding known functions with random phases, and applications to the theories of the shot effect and of light *Math. Proc. Camb. Phil. Soc.* **32** 580–97

[52] Chen F F 1984 *Introduction to Plasma Physics and Controlled Fusion* 2nd edn vol 1 (New York: Plenum Press)

[53] Chen F F 1965 Resistive overstabilities and anomalous diffusion *Phys. Fluids* **8** 912–9

[54] Pécseli H L 2012 *Waves and Oscillations in Plasmas* (London: Taylor and Francis)